Journal of the Egyptian Mathematical Society

ORIGINAL RESEARCH Open Access

Mixed convection flow of nanofluid with Hall and ion-slip effects using spectral relaxation method

Wubshet Ibrahim[1*] and Temesgen Anbessa[2]

* Correspondence: wubshetib@yahoo.com
[1]Department of Mathematics, Ambo University, Ambo, Ethiopia
Full list of author information is available at the end of the article

Abstract

In this article, the Hall and ion-slip effects on a mixed convection flow of an electrically conducting nanofluid over a stretching sheet in a permeable medium have been discussed. Using the similarity transformations, the partial differential equations corresponding to the momentum, energy, and concentration equations are transformed to a system of nonlinear ordinary differential equations which are solved numerically using a spectral relaxation method (SRM). The effects of significant parameters on the velocities, temperature, and concentration profiles are analyzed graphically. Moreover, the results of the skin friction coefficients, local Nusselt number, and Sherwood number are determined numerically. The results of the analysis showed that the velocity profile in the flow direction increases with an increase in mixed convection parameter λ, Hall parameter β_h, and ion-slip parameter β_i, and it decreases with an increase in the magnetic parameter M. Furthermore, temperature and concentration profiles decrease as the mixed convection parameter λ and buoyancy ratio Nr increase. It is also observed that the skin friction coefficients, local Nusselt number, and Sherwood number increase with an increase in the Hall parameter β_h, mixed convection parameter λ, and buoyancy ratio Nr.

Keywords: Mixed convection, Nanofluid, Hall and ion-slip effects, SRM

Introduction

Recently, the study of convection and heat transfer in the presence of nanofluid has obtained significant attention because of its wide applications in science, engineering, and industry. Some of these applications are welding equipment, power generating systems, cooling of nuclear reactor, automobile engines, and heat exchanging in electronics devices. The concept of nanofluid was first commenced by Choi [1] to refer to the fluids with suspended nanoparticles (1–100 nm). The suspended nanoparticles assist to enhance the thermal conductivity of the fluid. The effects of various governing parameters on heat and mass transfer of nanofluid flow through different geometries were studied by different scholars ([2–10]). Li et al. [11] numerically modeled electrohydrodynamic nanoparticle flow using control volume-based finite element method. Ramzan et al. [12] analyzed the aqueous-based nanofluid flow containing carbon nanotubes past a vertical cone through a porous medium with entropy generation and thermal radiation. Bilal and Ramzan [13] discussed unsteady two-dimensional flow of mixed convection and nonlinear thermal radiation in the presence of water-based carbon nanotubes over the vertically convected stretched sheet embedded in a Darcy-Forchheimer porous media using Saffman's proposed model for the suspension of fine dust particles in the nanofluid. Lu et al. [14] scrutinized a thin film flow of a nanofluid consisting of single and multi-walled carbon nanotubes with Cattaneo-Christov heat flux and entropy generation. Suleman et al. [15] studied the impacts of Newtonian heating and homogeneous–heterogeneous reactions on the flow of silver-water nanofluid past a nonlinear stretched cylinder with MHD and nonlinear thermal radiation. Suleman et al. [16] extended the work of Suleman et al. [15] by incorporating viscous dissipation, heat generation/absorption and joule heating effects. Madhu et al. [17] studied the boundary layer flow and heat transfer of a power-law non-Newtonian nanofluid past a nonlinearly stretching sheet. Madhu and Kishan [18] numerically investigated MHD mixed convection flow of heat and mass transfer stagnation-point flow of a non-Newtonian power-law nanofluid towards a stretching surface in the presence of thermal radiation using finite element method. Macha et al. [19] analyzed the MHD boundary layer flow of a viscous, incompressible and electrically conducting non-Newtonian nanofluid obeying power-law model over a nonlinear stretching sheet under the effect of thermal radiation with heat source/sink. Alebraheem and Ramzan [20] studied the heat and mass transfer of Casson nanofluid flow containing gyrotactic microorganisms past a swirling cylinder. Farooq et al. [21] described the static wedge flow of non-viscous Maxwell nanofluid using BVPh2.0 solver. Farooq et al. [22] analyzed the effects of thermophoretic and Brownian motion on MHD non-Newtonian Maxwell fluid with nanomaterials over an exponentially stretching surface using Buongiorno model. Macha et al. [23] investigated the MHD boundary layer flow of Sisko nanofluid flow past a wedge.

Mixed convection flows got a significant consideration because of its numerous technological and industrial applications. Aman and Ishak [24] numerically considered the effects of buoyancy force and convective surface boundary condition on mixed convection flow near a resistant vertical plate using shooting technique. Mahanthesh et al. [25] numerically investigated the influences of buoyancy force, nanoparticles, chemical reaction, and heat source/sink on combined forced and free convection flow of an electrically conducting water-based Cu-nanofluid past a moving/stationary vertical plate using Laplace transform method. The impacts of different governing parameters on mixed convection flow of nanofluid past stretching surfaces were studied by ([26–28]). Most recently, Khan and Rasheed [29] scrutinized magnetohydrodynamic (MHD) combined natural and forced convection flow of the Maxwell nanofluid with magnetic field and buoyancy force effects.

The Hall and ion-slip impacts are important under the existence of strong magnetic field because of the significant effect they have on the magnitude and direction of the electric current density and the magnetic force term. Hence, in numerous physical circumstances, it is necessary to incorporate the impact of Hall current and ion-slip terms in the MHD equations. The impacts of Hall and ion-slip parameters on combined forced and free convection flow of an electrically conducting Casson fluid were numerically analyzed using homotopy analysis method by Reddy et al. [30]. Moreover, Reddy et al. [31] analyzed the effects of Hall and ion-slip effects on combined forced and free convection flow of an electrically conducting Newtonian fluid using Adomian decomposition method. The Hall and ion-slip effects on mixed convection flow of an electrically conducting nanofluid through different geometries were discussed by ([32–35]). Motsa and Shateyi [36] numerically analyzed the effects of Hall and ion-slip currents on magnetomicropolar fluid flow with suction/injection using the spectral linearization method. Moreover, using shooting method, Bilal et al. [37] extended the work of Motsa and Shateyi [36] with the inclusion of nanoparticles neglecting the effect of chemical reaction. The Hall and ion-slip effects on unsteady MHD Couette flow of an electrically conducting fluid has been analytically discussed using Laplace transform method by Ghara et al. [38].

Ali et al. [39] have studied the effect of Hall current on MHD mixed convection flow over a stretched vertical flat plate. However, they did not consider ion-slip and permeability effects. Thus, the objective of the present study is to investigate the effects of Hall and ion-slip parameter on mixed convection flow of nanofluid past a porous stretching sheet. Therefore, the inclusion of the effects of ion-slip and permeability parameters in the presence of mass transfer makes this study a novel one. The governing equations are solved numerically using the SRM. This numerical method is chosen since its accuracy is high and the MATLAB program for the problem is manageable (see: Motsa and Makukula [40], Shateyi and Marewo [41], Shateyi and Marewo [42]). The fluid model considered in this study is solved numerically and hence will present an approximated solution. The other limitation of this flow problem is that the nanoparticle volume fraction is neglected.

Mathematical formulation

The study considered a laminar mixed convection flow of a viscous, incompressible, and electrically conducting nanofluid past a vertical linearly stretching sheet through a permeable medium with velocity $V_w(x)$ in the direction of x-axis. A strong uniform magnetic field M_0 is applied in the way along y-axis as shown in Fig. 1. As a result of this strong magnetic field force, the electrically conducting fluid has the Hall and ion-slip effects which generate a cross-flow in the z-direction, and thus, the flow becomes three dimensional. The induced magnetic field can be ignored in contrast with the applied magnetic field on the presumption that the flow is steady and the magnetic Reynolds number is very small. The mixed convection flow is caused by the buoyancy

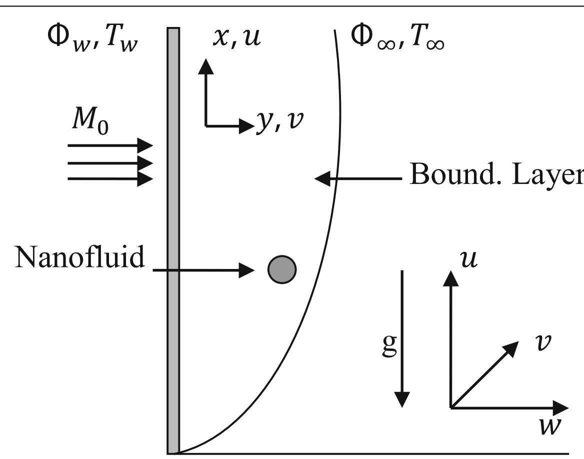

Fig. 1 Physical representation of the flow problem

forces. Further, all the fluid properties are understood to be constant except for density variations in the buoyancy force term. By applying the Boussinesq approximations with the above assumptions, the governing equations of continuity, momentum, energy, and concentration equations for the considered flow problem are ([35, 37, 38]):

$$\frac{\partial u}{\partial x}+\frac{\partial v}{\partial y}=0 \tag{1}$$

$$u\frac{\partial u}{\partial x}+v\frac{\partial u}{\partial y}=\upsilon\frac{\partial^2 u}{\partial y^2}-\frac{\sigma M_0^2}{\rho\left(\beta^2+\beta_h^2\right)}\left(\beta u+\beta_h w\right) + \mathrm{g}[\mathrm{B_T}(\mathrm{T}-\mathrm{T}_\infty)+\mathrm{B_C}(\Phi-\Phi_\infty)]-\frac{\nu}{\kappa}u \tag{2}$$

$$u\frac{\partial w}{\partial x}+v\frac{\partial w}{\partial y}=\upsilon\frac{\partial^2 w}{\partial y^2}+\frac{\sigma M_0^2}{\rho\left(\beta^2+\beta_h^2\right)}\left(\beta_h u-\beta w\right)-\frac{\nu}{\kappa}w \tag{3}$$

$$u\frac{\partial T}{\partial x}+v\frac{\partial T}{\partial y}=\alpha\frac{\partial^2 T}{\partial y^2}+\gamma\left[D_B\frac{\partial T}{\partial y}\frac{\partial \Phi}{\partial y}+\frac{D_T}{T_\infty}\left(\frac{\partial T}{\partial y}\right)^2\right] \tag{4}$$

$$u\frac{\partial \Phi}{\partial x}+v\frac{\partial \Phi}{\partial y}=D_B\frac{\partial^2 \Phi}{\partial y^2}+\frac{D_T}{T_\infty}\frac{\partial^2 T}{\partial y^2} \tag{5}$$

where (u, v, w) are the fluid velocity components along the (x, y, z) coordinates, μ is the dynamic viscosity, ρ is the density, ν is the kinematic viscosity, g is the acceleration due to gravity, T and Φ are the fluid temperature and concentration, respectively, T_∞ and ϕ_∞ are the ambient temperature and concentration, respectively, B_T is the coefficient of thermal expansion, B_C is the solutal coefficient of expansion, σ is the electrical conductivity, M_0 is the constant magnetic field applied normal to the surface, β_h is the Hall parameter, β_i is the ion-slip parameter, $\beta = 1 + \beta_h\ \beta_i$ is a constant, κ is the permeability of the porous medium, α is the thermal diffusivity, $(\rho\Phi)_p$ is the heat capacity of the nanoparticle, γ is the ratio of the effective heat capacity of nanoparticle material to the heat capacity of the fluid, D_B the Brownian diffusion coefficient, and D_T the thermophoresis diffusion coefficient.

The corresponding boundary conditions are:

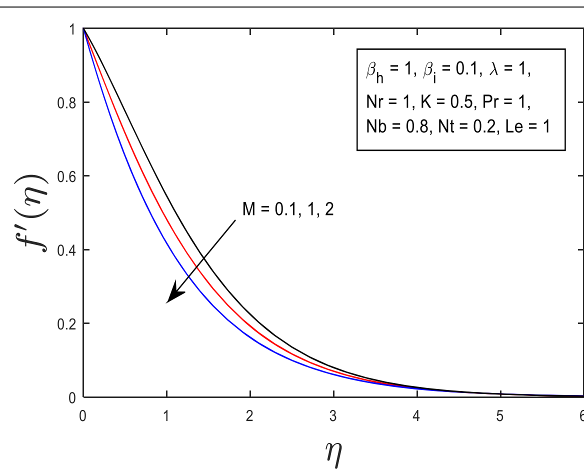

Fig. 2 Graph of velocity for various values of *M*

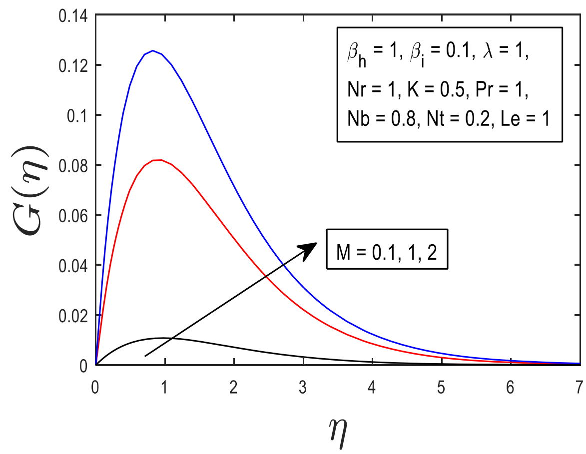

Fig. 3 Graph of cross flow velocity for various values of *M*

$$\begin{gathered} u = V_w(x) = Ax, v = w = 0, \\ T = T_w(x) = T_\infty + Bx, \\ \Phi = \Phi_w(x) = \Phi_\infty + Cx \quad at\ y = 0, \\ u \to 0, w \to 0, T \to T_\infty, \\ \Phi \to \Phi_\infty, \qquad as\ y \to \infty, \end{gathered} \tag{6}$$

where A, C (>0) and B are constants, and $T_w(x)$ and $\Phi_w(x)$ are variable surface temperature and concentration, respectively. Moreover, $B > 0$ denotes heated plate and $B < 0$ denotes cooled plate.

Let us establish the similarity transformations ([39, 43])

$$\begin{aligned} &\eta = \left(\frac{A}{\nu}\right)^{1/2} y, \qquad \psi = (A\nu)^{1/2} x f(\eta), \\ &w = AxG(\eta), \qquad \theta(\eta) = \frac{T - T_\infty}{T_w - T_\infty}, \\ &\varphi(\eta) = \frac{\Phi - \Phi_\infty}{\Phi_w - \Phi_\infty} \end{aligned} \tag{7}$$

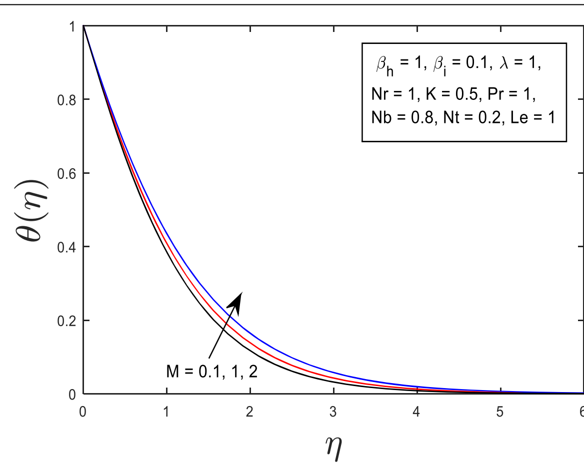

Fig. 4 Graph of temperature for various values of *M*

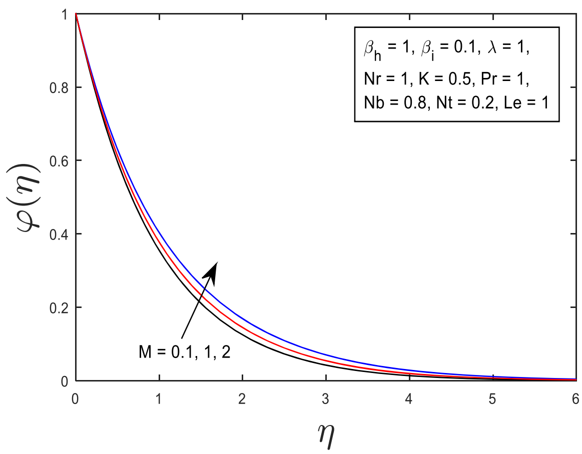

Fig. 5 Graph of concentration for various values of *M*

to obtain similarity solutions of Eqs. (1)–(5) subject to the boundary conditions (6), where the stream function $\psi(x, y)$ is defined as:

$$u = \frac{\partial \psi}{\partial y}, v = -\frac{\partial \psi}{\partial x}. \tag{8}$$

Substituting Eqs. (7) into Eqs. (2)–(5), the following ordinary differential equations are obtained:

$$f''' + ff'' - \left(f'\right)^2 - \frac{M}{(\beta^2 + \beta_h^2)}\left(\beta f' + \beta_h G\right) + \lambda(\theta + Nr\varphi) - Kf' = 0 \tag{9}$$

$$G'' + fG' - f'G + \frac{M}{(\beta^2 + \beta_h^2)}\left(\beta_h f' - \beta G\right) - KG = 0 \tag{10}$$

$$\theta'' + Pr\left(f\theta' - f'\theta + Nb\theta'\varphi' + Nt\theta'^2\right) = 0 \tag{11}$$

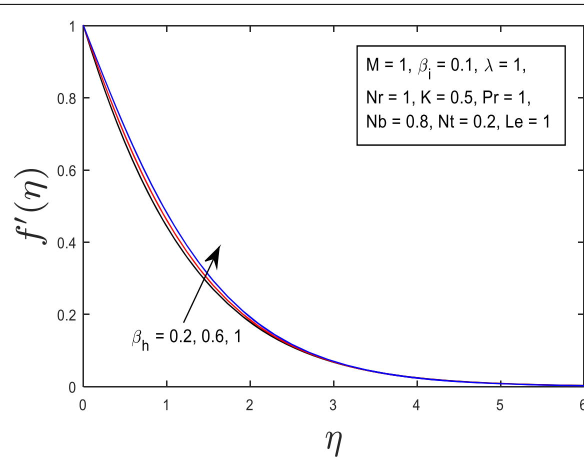

Fig. 6 Graph of velocity for various values of β_h

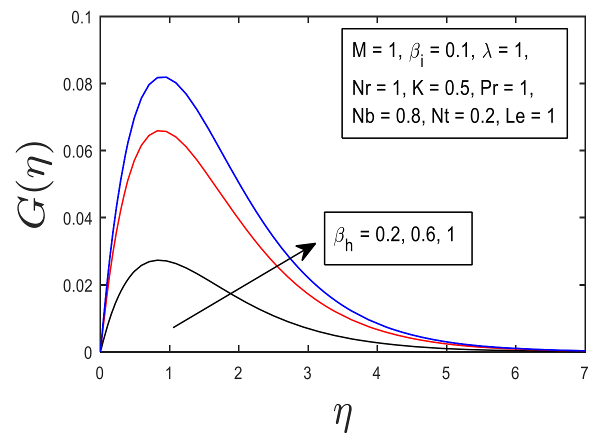

Fig. 7 Graph of cross flow velocity for various values of β_h

$$\varphi'' + PrLe\left(f\varphi' - f'\varphi\right) + \frac{Nt}{Nb}\theta'' = 0 \quad (12)$$

with the transformed boundary conditions:

$$\begin{gathered} f(0) = 0, \quad f'(0) = 1, \quad G(0) = 0, \\ \theta(0) = 1, \quad \varphi(0) = 1, \\ f' \to 0, G \to 0, \theta \to 0, \\ \varphi \to 0, as \quad \eta \to \infty, \end{gathered} \quad (13)$$

where $M = \sigma M_0^2/\rho A$ is the magnetic parameter, $\lambda = Gr_x/\ Re_x^2$ is the constant mixed convection parameter where $Gr_x = gB_T(T_w - T_\infty)x^3/\nu^2$ is the local Grashof number, and $Re_x = Ax^2/\nu$ is the local Reynolds number, $Nr = B_C(\Phi_w - \Phi_\infty)/B_T(T_w - T_\infty)$ is the buoyancy ratio, $K = \nu/A\kappa$ is the permeability parameter, $Pr = \nu/\alpha$ is the Prandtl number, $Nb = \gamma D_B(\Phi_w - \Phi_\infty)/\nu$ is the Brownian motion parameter, $Nt = \gamma D_T(T_w - T_\infty)/\nu T_\infty$ is the thermophoresis parameter, $Le = \alpha/D_B$ is the Lewis number, and $\gamma = (\rho\Phi)_p/(\rho\Phi)_f$ is the ratio between the heat capacity of the nanoparticle material and heat capacity of the fluid.

The physical quantities of interest are the skin friction coefficients C_{fx} and C_{fz}, the local Nusselt number Nu_x, and the Sherwood number Sh_xwhich are defined as follows:

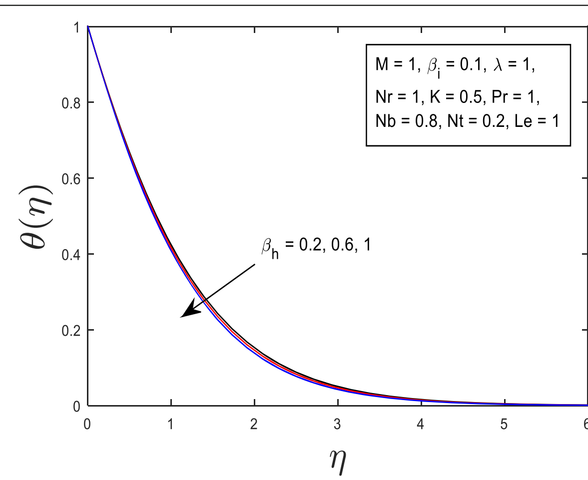

Fig. 8 Graph of temperature for various values of β_h

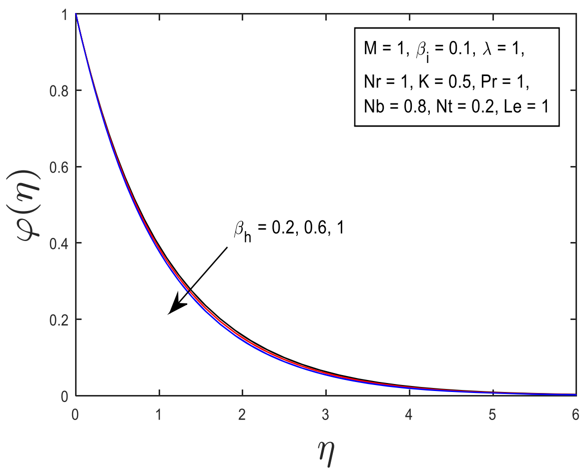

Fig. 9 Graph of concentration for various values of $\boldsymbol{\beta_h}$

$$C_{fx} = \frac{2\tau_{wx}}{\rho V_w^2}, \quad C_{fz} = \frac{2\tau_{wz}}{\rho V_w^2}, \quad Nu_x = \frac{xq_w}{k(T_W - T_\infty)}, \quad Sh_x = \frac{x\mathrm{j}_m}{D_B(\Phi_W - \Phi_\infty)} \tag{14}$$

where τ_{wx} and τ_{wz} are the wall shear stresses in the directions of x and z, respectively, q_w is the surface heat flux, and j_m is the surface mass flux, which are given by

$$\begin{aligned} \tau_{wx} &= \mu\left(\frac{\partial u}{\partial y}\right)\Bigg|_{y=0}, \tau_{wz} = \mu\left(\frac{\partial w}{\partial y}\right)\Bigg|_{y=0}, \\ q_w &= -k\left(\frac{\partial T}{\partial y}\right)\Bigg|_{y=0}, \\ \mathrm{j}_m &= -D_B\left(\frac{\partial \Phi}{\partial y}\right)\Bigg|_{y=0} \end{aligned} \tag{15}$$

From Eqs. (7) and (14), we get

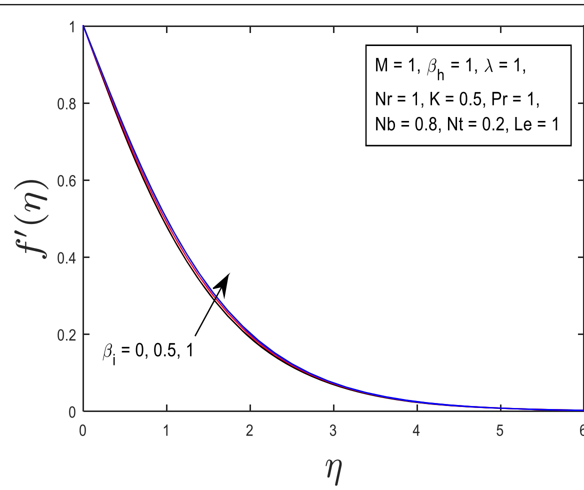

Fig. 10 Graph of velocity for various values of $\boldsymbol{\beta_i}$

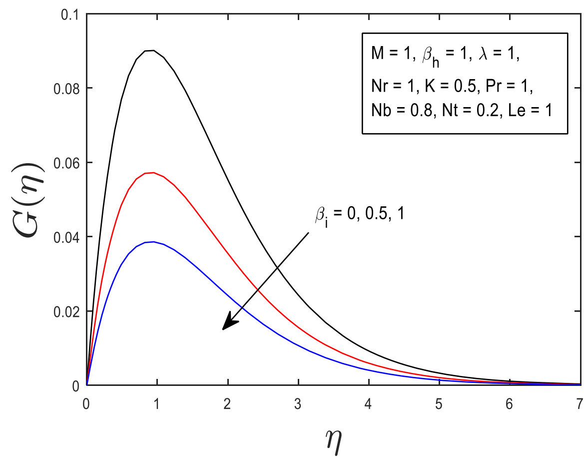

Fig. 11 Graph of cross flow velocity for various values of β_i

$$C_{fx} = \frac{2}{\sqrt{Re_x}} f''(0), \quad C_{fz} = \frac{2}{\sqrt{Re_x}} G'(0), \quad Nu_x = -\sqrt{Re_x}\,\theta'(0),$$
$$Sh_x = -\sqrt{Re_x}\,\varphi'(0). \tag{16}$$

Method of solution

The spectral relaxation method (SRM) is used to solve the system of nonlinear ordinary differential Eqs. (9)–(12) subject to the boundary conditions (13). To implement the SRM, the order of the momentum Eq. (9) is reduced to second order introducing the transformation $f' = H$ so that $f'' = H'$ *and* $f''' = H''$. Hence, Eqs. (9)–(12) and the boundary conditions (13) can be transformed as follows:

$$f' = H \tag{17}$$

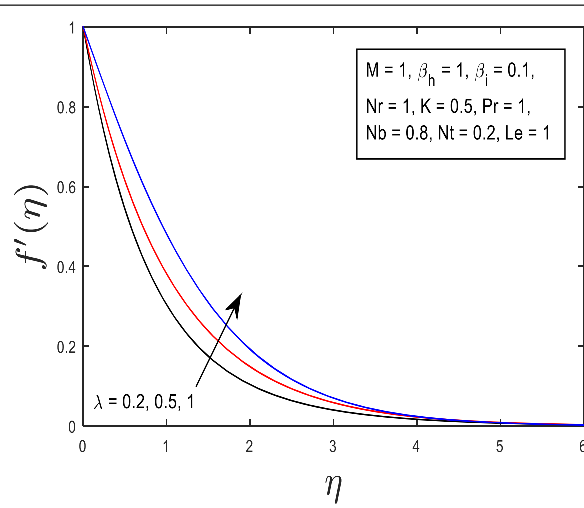

Fig. 12 Graph of velocity for various values of **λ**

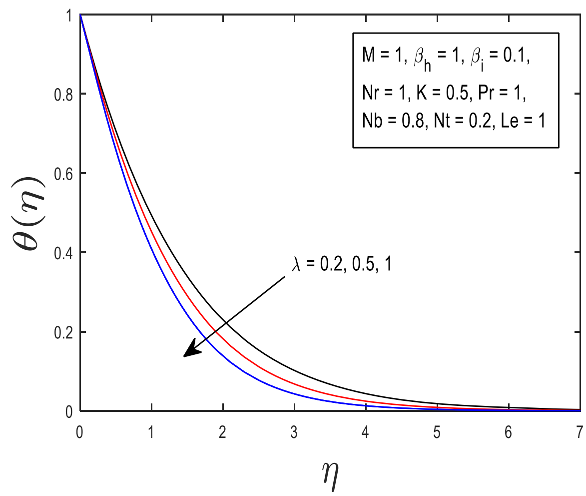

Fig. 13 Graph of temperature for various values of **λ**

$$H^{''}+fH^{'}-(H)^2-\frac{M}{(\beta^2+\beta_h^2)}(\beta H+\beta_h G)+\lambda(\theta+Nr\varphi)-KH=0 \quad (18)$$

$$G^{''}+fG^{'}-HG+\frac{M}{(\beta^2+\beta_h^2)}(\beta_h H-\beta G)-KG=0 \quad (19)$$

$$\theta^{''}+\ Pr\left(f\theta^{'}-H\theta+Nb\theta^{'}\varphi^{'}+Nt\theta^{'2}\right)=0 \quad (20)$$

$$\varphi^{''}+PrLe\left(f\varphi^{'}-H\varphi\right)+\frac{Nt}{Nb}\theta^{''}=0 \quad (21)$$

subject to the boundary conditions

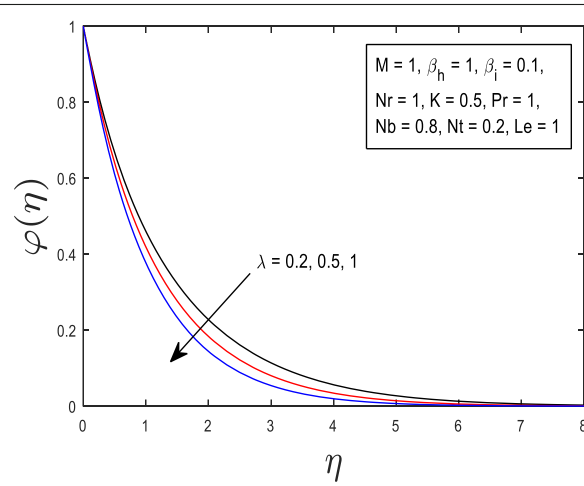

Fig. 14 Graph of concentration for various values of **λ**

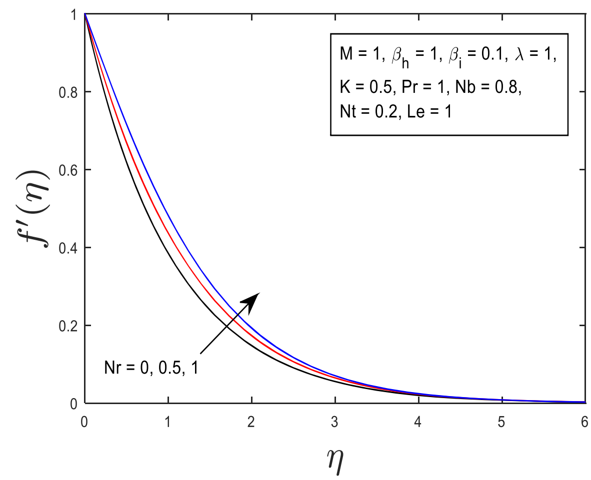

Fig. 15 Graph of velocity for various values of Nr

$$\begin{gathered} f(0)=0, H(0)=1, G(0)=0, \\ \theta(0)=1, \quad \varphi(0)=1, \\ H \to 0, G \to 0, \theta \to 0, \varphi \to 0 \\ as \quad \eta \to \infty. \end{gathered} \tag{22}$$

Detail rules of the SRM can be found in ([40–42]). The resulting iteration scheme in SRM for Eqs. (17)–(22) can be written as follows:

$$f'_{r+1} = H_r \tag{23}$$

$$H''_{r+1} + f_{r+1}H'_{r+1} - H_r^2 - \frac{M}{(\beta^2+\beta_h^2)}\left(\beta H_{r+1} + \beta_h G_r\right) + \lambda(\theta_r + Nr\varphi_r) - KH_{r+1} = 0 \tag{24}$$

$$G''_{r+1} + f_{r+1}G'_{r+1} - H_{r+1}G_{r+1} + \frac{M}{(\beta^2+\beta_h^2)}\left(\beta_h H_{r+1} - \beta G_{r+1}\right) - KG_{r+1} = 0 \tag{25}$$

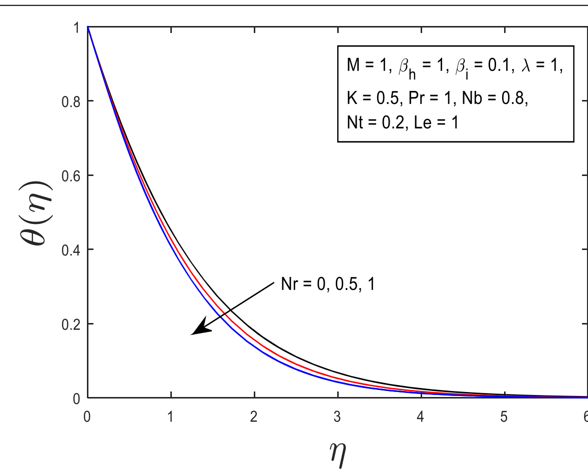

Fig. 16 Graph of temperature for various values of *Nr*

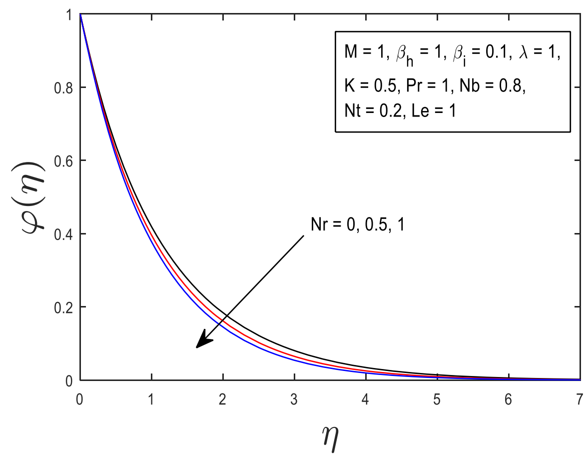

Fig. 17 Graph of concentration for various values of Nr

$$\theta''_{r+1} + \Pr\left(f_{r+1}\theta'_{r+1} - H_{r+1}\theta_{r+1} + Nb\theta'_{r+1}\varphi'_r + Nt\theta_r'^{\,2}\right) = 0 \tag{26}$$

$$\varphi''_{r+1} + PrLe\left(f_{r+1}\varphi'_{r+1} - H_{r+1}\varphi_{r+1}\right) + \frac{Nt}{Nb}\theta''_{r+1} = 0 \tag{27}$$

subject to the boundary conditions

$$\begin{array}{c} f_{r+1}(0) = 0, H_{r+1}(0) = 1, G_{r+1}(0) = 0, \\ \theta_{r+1}(0) = 1, \quad \varphi_{r+1}(0) = 1, \\ H_{r+1}\to 0, \quad G_{r+1}\to 0, \theta_{r+1}\to 0, \\ \varphi_{r+1}\to 0 \quad as \quad \eta\to\infty. \end{array} \tag{28}$$

In Eqs. (23)–(28), $r + 1$ and r denote the current and previous iteration, respectively. Implementing Chebyshev differentiation (Trefethen [44]) on iterative scheme defined by Eqs. (23)–(27), we obtain the following discrete form:

$$\boldsymbol{B}_1 \mathbf{f}_{r+1} = \boldsymbol{R}_1, \qquad f_{r+1}(\zeta_N) = 0 \tag{29}$$

$$\boldsymbol{B}_2 \mathbf{H}_{r+1} = \boldsymbol{R}_2, \qquad H_{r+1}(\zeta_N) = 1, \quad H_{r+1}(\zeta_0) = 0 \tag{30}$$

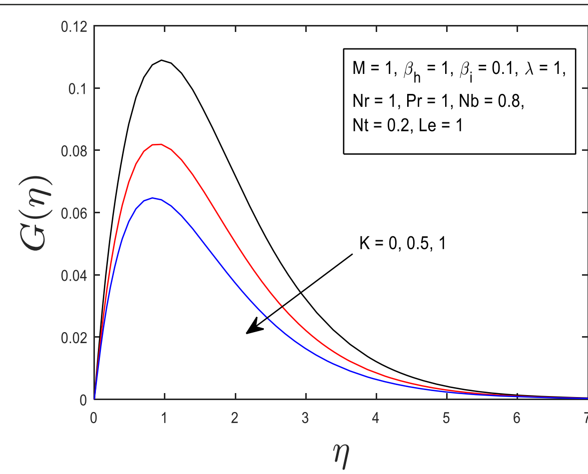

Fig. 18 Graph of cross flow profiles for various values of *K*

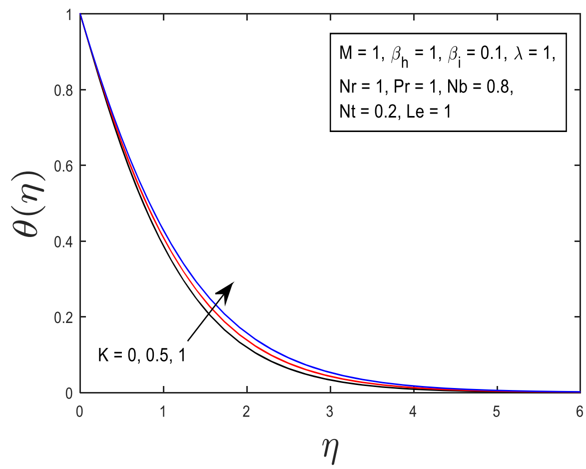

Fig. 19 Graph of temperature for various values of *K*

$$\boldsymbol{B_3}\mathbf{G}_{\mathrm{r+1}} = \mathbf{R_3}, \qquad G_{r+1}(\zeta_N) = 0, \quad G_{r+1}(\zeta_0) = 0 \tag{31}$$

$$\boldsymbol{B_4}\boldsymbol{\theta}_{\mathrm{r+1}} = \mathbf{R_4}, \qquad \theta_{r+1}(\zeta_N) = 1, \theta_{r+1}(\zeta_0) = 0 \tag{32}$$

$$\boldsymbol{B_5}\boldsymbol{\phi}\_\mathrm{r} + 1 = \mathbf{R_5}, \qquad \varphi_{r+1}(\zeta_N) = 1, \ \ \varphi_{r+1}(\zeta_0) = 0 \tag{33}$$

where

$$\boldsymbol{B_1} = \boldsymbol{D}, \qquad\qquad \boldsymbol{R}\_\mathbf{1} = H_r \tag{34}$$

$$\begin{aligned} B_2 &= D^2 + \ \mathrm{diag}\left(f_{r+1}\right)D - \left(\frac{M\beta}{\beta^2 + \beta_h^2} + K\right)\mathbf{I}, \\ \mathbf{R}\_2 &= H_r^2 + \frac{M\beta_h}{\left(\beta^2 + \beta_h^2\right)} G_r - \lambda(\theta_r + Nr\varphi_r) \end{aligned} \tag{35}$$

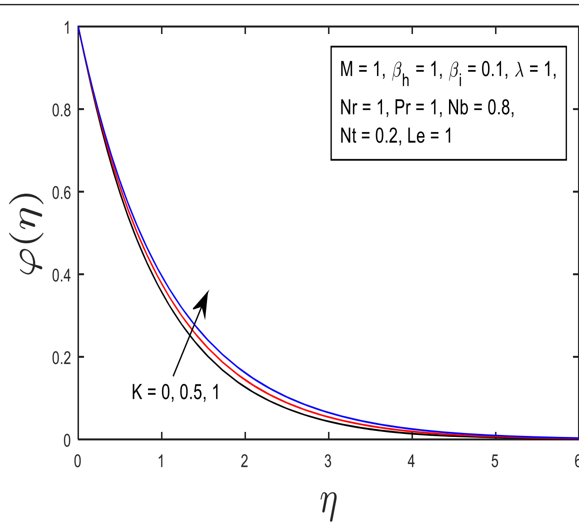

Fig. 20 Graph of concentration for various values of *K*

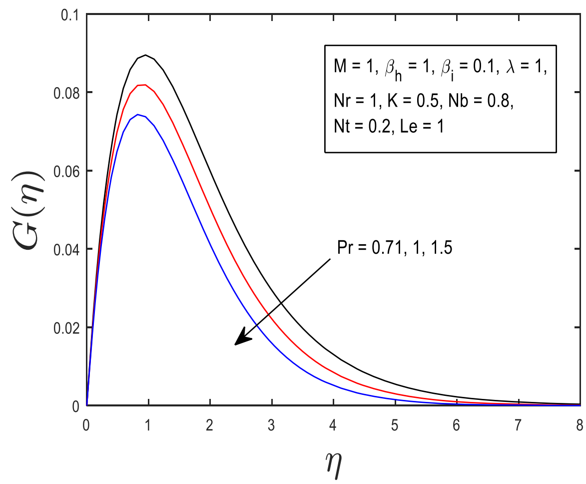

Fig. 21 Graph of cross flow velocity for various values of Pr

$$B_3 = D^2 + \operatorname{diag}(f_{r+1})D - \operatorname{diag}(H_{r+1}) - \left(\frac{M\beta}{\beta^2+\beta_h^2}+K\right)\mathbf{I},$$
$$R\_3 = -\frac{M\beta_h}{\beta^2+\beta_h^2}H_{r+1} \tag{36}$$

$$B_4 = D^2 + Pr\ \operatorname{diag}\left(f_{r+1}+Nb\varphi_r'\right)D - Pr\ \operatorname{diag}(H_{r+1}),$$
$$R\_4 = -PrNt\theta_r'^{\,2} \tag{37}$$

$$B_5 = D^2 + Le(\ \operatorname{diag}(f_{r+1})D - Le\ \operatorname{diag}(H_{r+1}),$$
$$R\_5 = -\frac{Nt}{Nb}\theta_{r+1}'' \tag{38}$$

where $\boldsymbol{D} = 2D/\eta_\infty$, D is the Chebyshev differentiation matrix, and $\mathbf{I}$ is the identity matrix of size $(N+1)\times(N+1)$. The decoupled Eqs. (29)–(33) can be solved independently by choosing a proper initial guesses:

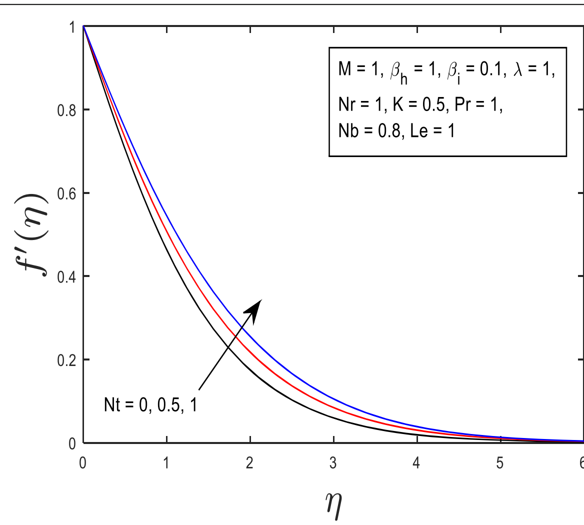

Fig 22 Graph of velocity for various values of *Nt*

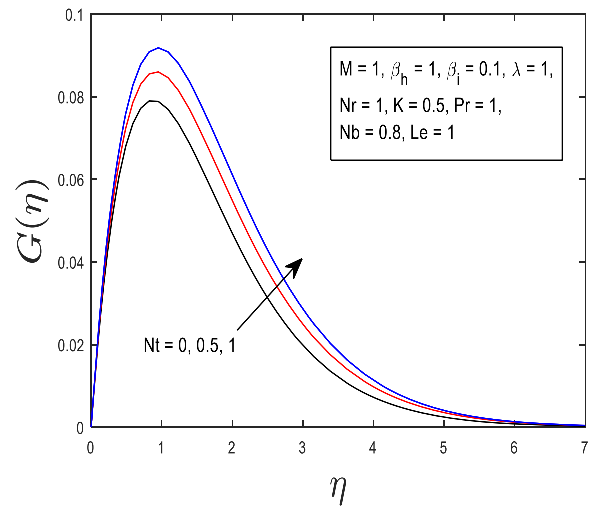

Fig. 23 Graph of cross flow velocity for various values of Nt

$$
\begin{aligned}
f_0(\eta) &= 1- \exp(-\eta),\\
G_0(\eta) &= \eta \exp(-\eta),\\
\theta_0(\eta) = \phi\_0(\eta) &= \exp(-\eta).
\end{aligned}
\tag{39}
$$

Results and discussions

The nonlinear ordinary differential Eqs. (9) to (12) with respect to the boundary conditions (13) are solved numerically using SRM. The numerical solutions are obtained for velocities, temperature, and concentration profiles for different values of governing parameters. The graphical representations of the numerical results are shown in Figs. 2, 3, 4, 5, 6, 7, 8, 9, 10, 11, 12, 13, 14, 15, 16, 17, 18, 19, 20, 21, 22 and 23. Unless otherwise stated, the numerical values for the parameters are taken to be fixed as $M = \beta_h = \lambda = Nr = Pr = Le = 1.0$, $\beta_i = 0.1$, $K = 0.5$, $Nb = 0.8$, and $Nt = 0.2$.

The ranges of parameters used in the figures are $0.1 \le M \le 2.0$, $0.2 \le \beta_h \le 1.0$, $0.0 \le \beta_i \le 1.5$, $0.2 \le \lambda \le 1.0$, $0.0 \le Nr \le 1.0$, $0.0 \le K \le 1.0$, $0.71 \le Pr \le 1.5$, and $0.0 \le Nt \le 1.0$. For the authentication of the numerical method used, the results were compared with the previously obtained results for various values of parameters and it indicates an excellent accord as shown in Tables 1 and 2.

From Table 3, it is observed that the skin friction coefficient $-f''(0)$ in the x-direction increases with the increasing values of β_h, β_i, λ, Nr, and Nt, and it decreases for

Table 1 Comparison of $-\theta'(0)$ for various values of Pr when $M = \beta_h = \beta_i = \lambda = \mathrm{Nr} = K = \mathrm{Nb} = \mathrm{Nt} = \mathrm{Le} = \varphi = 0$

Pr	Ali et al. [39]	Ramzan et al. [43]	Grubka and Bobba [45]	Present results
0.01	0.0198	–	0.0197	0.01988750
0.72	0.8086	0.8086313	0.8086	0.80863151
1	1.0000	1.0000000	1.0000	1.00000000
3	1.9237	1.9359130	1.9237	1.92368259
10	3.7208	3.7215958	3.7207	3.72067428
100	12.3004	–	12.2940	12.29413922

Table 2 Comparison of $-f''(0)$ and $-\theta'(0)$ for different values of M with $\beta_h = 0, 2,\ \lambda = \Pr = 1$ and $\beta_i = \text{Nr} = K = \text{Nb} = \text{Nt} = \text{Le} = \varphi = 0$

M	Ali et al. [39]				Present results			
	$\beta_h = 0$		$\beta_h = 2$		$\beta_h = 0$		$\beta_h = 2$	
	$-f''(0)$	$-\theta'(0)$	$-f''(0)$	$-\theta'(0)$	$-f''(0)$	$-\theta'(0)$	$-f''(0)$	$-\theta'(0)$
0	0.5607	1.0873	0.5608	1.0873	0.560941	1.087206	0.560941	1.087206
0.01	0.5658	1.0863	0.5618	1.0871	0.565820	1.086269	0.561782	1.087072
0.04	0.5810	1.0833	0.5649	1.0865	0.581027	1.083262	0.564835	1.086452
0.25	0.6830	1.0630	0.5878	1.0816	0.683029	1.063010	0.587819	1.081601
1	1.0000	1.0000	0.6816	1.0591	1.000000	1.000000	0.681587	1.059134

increasing values of M and Nb. It is also noticed that the skin friction coefficient $G'(0)$ in the z-direction increases as M, β_h, λ, Nr, and Nt increase, and it decreases by increasing β_i and Nb. The table also shows that the local Nusselt number $-\theta'(0)$ increases with an increase in β_h, β_i, λ, and Nr, and it decreases with an increase in M, Nb, and Nt. Furthermore, the local Sherwood number $-\varphi'(0)$ increases as β_h, β_i, λ, Nr, and Nb increase and decreases as M and Nt increase.

Figures 2, 3, 4 and 5 show the effects of magnetic parameter M on the velocity $f'(\eta)$, cross flow velocity $G(\eta)$, temperature $\theta(\eta)$, and concentration $\varphi(\eta)$ profiles, respectively. The velocity profile $f'(\eta)$ decreases with an increase in the values of M, whereas the cross

Table 3 Numerical values of the skin friction coefficients $-f''(0)$ and $G'(0)$, local Nusselt number $-\theta'(0)$, and local Sherwood number $-\varphi'(0)$ for various values of M, β_h, β_i, λ, Nr, Nb, and Nt when $K = 0.5$, $Pr = 1$, and $Le = 1$ are fixed

M	β_h	β_i	λ	Nr	Nb	Nt	$-f''(0)$	$G'(0)$	$-\theta'(0)$	$-\varphi'(0)$
0.0	1.0	0.1	1.0	1.0	0.8	0.2	0.358052	0.000000	0.787875	1.022604
0.2	1.0	0.1	1.0	1.0	0.8	0.2	0.404568	0.054074	0.783140	1.014387
0.4	1.0	0.1	1.0	1.0	0.8	0.2	0.451324	0.104165	0.778270	1.005904
1.0	0.0	0.1	1.0	1.0	0.8	0.2	0.774312	0.000000	0.745503	0.950242
1.0	0.3	0.1	1.0	1.0	0.8	0.2	0.738252	0.121134	0.748909	0.955825
1.0	0.6	0.1	1.0	1.0	0.8	0.2	0.674238	0.196848	0.754994	0.965852
1.0	1.0	0.0	1.0	1.0	0.8	0.2	0.594820	0.258345	0.762577	0.978417
1.0	1.0	0.1	1.0	1.0	0.8	0.2	0.590784	0.234345	0.763224	0.979652
1.0	1.0	0.2	1.0	1.0	0.8	0.2	0.585817	0.212930	0.763922	0.980946
1.0	1.0	0.1	0.0	1.0	0.8	0.2	1.424897	0.174459	0.649559	0.776368
1.0	1.0	0.1	0.2	1.0	0.8	0.2	1.236853	0.192259	0.685824	0.845391
1.0	1.0	0.1	0.5	1.0	0.8	0.2	0.981128	0.211193	0.721370	0.908559
1.0	1.0	0.1	1.0	0.0	0.8	0.2	0.973008	0.211529	0.722476	0.909963
1.0	1.0	0.1	1.0	0.2	0.8	0.2	0.893654	0.216702	0.731814	0.926210
1.0	1.0	0.1	1.0	0.4	0.8	0.2	0.815937	0.221519	0.740447	0.941069
1.0	1.0	0.1	1.0	1.0	0.1	0.2	0.459690	0.251479	1.027856	-0.019822
1.0	1.0	0.1	1.0	1.0	0.4	0.2	0.582084	0.236050	0.889731	0.837193
1.0	1.0	0.1	1.0	1.0	0.8	0.2	0.590791	0.234344	0.763222	0.979651
1.0	1.0	0.1	1.0	1.0	0.8	0.0	0.616011	0.230279	0.788958	1.067908
1.0	1.0	0.1	1.0	1.0	0.8	0.2	0.590791	0.234344	0.763222	0.979651
1.0	1.0	0.1	1.0	1.0	0.8	0.4	0.567447	0.238062	0.738055	0.903053

flow velocity $G(\eta)$, temperature $\theta(\eta)$ and concentration $\varphi(\eta)$ profiles increase as M increases. As M increases, a drag force, called Lorentz force increases. Since this force opposes the flow of nanofluid, velocity in the flow direction decreases. Moreover, since an electrically conducting nanofluid with the strong magnetic field in the direction orthogonal to the flow are considered, an increase in M increases the force in the z-direction which results in an increase in the cross flow velocity profile $G(\eta)$.

Figures 6, 7, 8 and 9 illustrate the impacts of the Hall parameter β_h on the velocity $f'(\eta)$, cross flow velocity $G(\eta)$, temperature $\theta(\eta)$, and concentration $\varphi(\eta)$ profiles, respectively. It is observed that both the velocity $f'(\eta)$) and cross flow velocity $G(\eta)$ profiles increase as β_h increases. But, the temperature and concentration profiles decrease with an increase in β_h as shown in Figs. 8 and 9. This is because the enclosure of Hall parameter decreases the resistive force caused by the magnetic field due to its effect of reducing the effective conductivity. Hence, the velocity component increases as the Hall parameter increases.

The influences of the ion-slip parameter β_i on the velocity $f'(\eta)$ and cross flow velocity $G(\eta)$ profiles are depicted in Figs. 10 and 11, respectively. The effective conductivity increases with an increase in ion-slip parameter, consecutively damping force decreases on the velocity component in the direction of the flow, and hence, the velocity component increases in the flow direction. Thus, Fig. 10 shows that the velocity profile $f'(\eta)$ increases insignificantly as β_i increases. Conversely, in Fig. 11, a rise in β_i leads to a decline in the cross flow velocity profile $G(\eta)$.

Figures 12, 13 and 14 disclose the impacts of mixed convection parameter λ on the velocity $f'(\eta)$, temperature $\theta(\eta)$, and concentration $\varphi(\eta)$ profiles. It is deducted that as λ enhances, the velocity profile $f'(\eta)$ rises and conversely, the temperature $\theta(\eta)$ and concentration $\varphi(\eta)$ profiles diminish. This is due to the fact that a rise in λ (>0) accelerates the fluid's flow for $g > 0$ and hence results in an increase in fluid's velocity. Furthermore, fluids having larger value of λ have lower thermal diffusivity which reduces the energy capability and the thermal boundary layer thickness.

The effects of the buoyancy ratio Nr on the velocity $f'(\eta)$, temperature $\theta(\eta)$, and the concentration $\varphi(\eta)$ profiles are shown in Figs. 15, 16 and 17, respectively. Figure 15 reveals that the velocity profile $f'(\eta)$ increases as Nr increases, while in Figs. 16 and 17, the temperature and concentration $\varphi(\eta)$ profiles decrease as Nr increases. The fact is that a rise in Nr decreases fluid's viscosity. Hence, the result follows.

Figures 18, 19 and 20 demonstrate the effects of the permeability parameter K on the cross flow velocity $G(\eta)$, temperature $\theta(\eta)$, and concentration $\varphi(\eta)$ profiles, respectively. From Fig. 18, it is noticed that as K rises, the cross flow velocity profile diminishes. A rise in resistance against the fluid flow is examined by increasing the thickness of permeable medium which results in a decrease in fluid velocity. In addition, a rise in permeability parameter enhances the thickness of the boundary layer of temperature and concentration. Thus, the temperature and concentration profiles enhance with an increase in K as shown in the Figs. 19 and 20.

Figure 21 divulges the effects of the prandtl number Pr on the cross flow velocity profile $G(\eta)$. Since fluids having a larger Pr have lower thermal diffusivity, the cross flow velocity profile $G(\eta)$ decreases as the values of Pr increases.

The influence of the thermophoresis parameter Nt on the velocity $f'(\eta)$ and cross flow velocity $G(\eta)$ profiles are depicted in Figs. 22 and 23, respectively. As it is observed, both flow velocity and cross flow velocity profiles increase as Nt increases. This is for the reason that the temperature gradient generates a thermophoresis force, and it creates a fast flow away from the stretching sheet. Hence, the velocity profiles increase with an increase in Nt.

Conclusions

A numerical study of a steady mixed convection flow of an electrically conducting nanofluid over a linearly stretching sheet in the presence of Hall and ion-slip effects has been carried out. With the help of similarity transformations the governing partial differential equations for momentum, energy, and concentration equations were reduced to couple nonlinear ordinary differential equations which were then solved numerically using spectral relaxation method. The effects of different governing parameters on the velocities, temperature, and concentration profiles are studied and revealed the following results:

❖ The velocity profile $f'(\eta)$ increases with an increase in β_h, β_i, λ, Nr, and Nt and decreases with an increase in M.

❖ As M, β_h, and Nt increase, the cross flow velocity profile $G(\eta)$ increases.

❖ As β_i, K, and Pr increase, the cross flow velocity profile $G(\eta)$ decreases.

❖ The temperature profile $\theta(\eta)$ increases as M and K increase and decreases as β_h, λ, and Nr increase.

❖ The concentration profile $\varphi(\eta)$ increases as M and K increase and decreases with an increase in β_h, λ, and Nr.

Nomenclature

A, B, C Constants
x, y, z Cartesian coordinates
u, v, w Velocity components
$V_w(x)$ Velocity of the stretching sheet
M_0 Constant magnetic field strength
g Acceleration due to gravity
T Fluid temperature
T_w Surface temperature
T_∞ Ambient temperature
Φ Concentration of fluid
Φ_w Surface concentration
Φ_∞ Ambient concentration
μ Dynamic viscosity of the fluid
ρ Density of fluid
ν Kinematic viscosity of the fluid
λ Mixed convection parameter
α Thermal diffusivity
σ Electrical conductivity
β_h Hall parameter
β_i Ion-slip parameter
B_T Solutal expansion coefficient
B_C Thermal expansion coefficient
κ Permeability of porous medium
η Dimensionless similarity variable

ψ Stream function
θ Dimensionless temperature
φ Dimensionless concentration
D_B Brownian diffusion coefficient
D_T Thermophoresis diffusion coefficient
M Magnetic parameter
Gr_x Local Grashof number
Re_x Local Reynolds number
Nr Buoyancy ratio
K Permeability parameter
Pr Prandtl number
Le Lewis number
Nb Brownian motion parameter
Nt Thermophoresis parameter
f, G Dimensionless stream functions
$(\rho\Phi)_p$ Effective heat capacity of a nanoparticle
$(\rho\Phi)_f$ Heat capacity of the fluid
τ_{wx} Wall shear stresses in the x-direction
τ_{wz} Wall shear stresses in the z-direction
C_{fx} Skin friction coefficient in x–direction
C_{fz} Skin friction coefficient in z–direction
Nu_x Local Nusselt number
Sh_x Local Sherwood number
q_w Surface heat flux
j_m Surface mass flux
Subscripts
f Fluid
p Nanoparticle
w Condition at the surface
∞ Ambient condition
Superscripts
' Differentiation w. r. t. η

Authors' contributions
All the authors have made substantive contributions to the article and assume full responsibility for its content. Both authors read and approved the final manuscript.

Funding
No fund for the conduction of this research.

Availability of data and materials
Data sharing is not applicable to this article as no datasets were generated or analyzed during the current study.

Competing interests
The authors declare that they have no competing interests.

Author details
[1]Department of Mathematics, Ambo University, Ambo, Ethiopia. [2]Department of Mathematics, Wollega University, Nekemte, Ethiopia.

Received: 29 July 2019 Accepted: 25 September 2019
Published online: 17 December 2019

References

1. Choi, S.U.S.: Enhancing thermal conductivity of fluids with nanoparticles. In: Proceedings of the ASME International Mechanical Engineering Congress and Exposition, vol. 66, pp. 99–105. ASME, FED 231/MD, San Francisco (1995)
2. Ittedi, S., Ramya, D., Joga, S.: MHD heat transfer of nanofluids over a stretching sheet with slip effects and chemical reaction. Int. J. of Lat. Eng. Res. Appl. **02**, 10–20 (2017)
3. Sreekala, B., Janardhan, K., Ramya, D., Shravani, I.: MHD boundary layer nanofluid flow of heat transfer over a nonlinear stretching sheet presence of thermal radiation and partial slip with suction. Glob. J. of Pure Appl. Math. **13**, 4927–4941 (2017)
4. Yohannes, K.Y., Shankar, B.: Heat and mass transfer in MHD flow of nanofluids through a porous media due to a stretching sheet with viscous dissipation and chemical reaction effects. Carib. J. Sci. Tech. **1**, 1–17 (2013)
5. Ibrahim, W.: Magnetohydrodynamic (MHD) boundary layer stagnation point flow and heat transfer of a nanofluid past a stretching sheet with melting. Prop. Power Res. **6**(3), 214–222 (2017) https://doi.org/10.1016/j.jppr.2017.07.002
6. Kasaeian, A., Azarian, R.D., Mahian, O., Kolsi, L., Chamkha, A.J., Wongwises, S., Pop, I.: Nanofluid flow and heat transfer in porous media: a review of the latest developments. Int. J. of Heat Mass Transf. **107**, 778–791 (2017) https://doi.org/10.1016/j.ijheatmasstransfer.2016.11.074
7. Ittedi, S., Ramya, D., Joga, S.: Partial slip effect of MHD boundary layer flow of nanofluids and radiative heat transfer over a permeable stretching sheet. Glob. J. of Pure Appl. Math. **13**(7), 3083–3103 (2017)
8. Sulochana, C., Samrat, S.P., Sandeep, N.: Thermal radiation effect on MHD nanofluid flow over a stretching sheet. Int. J. of Eng. Res. in Africa. **23**, 89–102 (2016). https://doi.org/10.4028/www.scientific.net/JERA.23.89
9. Haroun, N.A.H., Mondal, S., Sibanda, P.: Unsteady natural convective boundary-layer flow of MHD nanofluid over a stretching surface with chemical reaction using the spectral relaxation method: a revised model. Proc. Eng. **127**, 18–24 (2015). https://doi.org/10.1016/j.proeng.2015.11.317
10. Reddy, C.H.A., Shankar, B.: Magnetohydrodynamics stagnation point flow of a nanofluid over an exponentially stretching sheet with an effect of chemical reaction, heat source and suction/injunction. World. J. Mech. 5, 211 – 221 (2015). https://doi.org/10.4236/wjm.2015.511020
11. Li, Z., Ramzan, M., Shafee, A., Saleem, S., Al-Mdallal, Q.M., Chamkha, A.J.: Numerical approach for nanofluid transportation due to electric force in a porous enclosure. Micro. Tech. **25**(6), 2501–2514 (2019)
12. Ramzan, M., Mohammad, M., Howari, F., Chung, J.D.: Entropy analysis of carbon nanotubes based nanofluid flow past a vertical cone with thermal radiation. Entropy. **21**(7), 1–17 (2019). https://doi.org/10.3390/e21070642
13. Bilal, M., Ramzan, M.: Hall current effect on unsteady rotational flow of carbon nanotubes with dust particles and nonlinear thermal radiation in Darcy–Forchheimer porous media. J. of Therm. Analy. Calori. 1–11 (2019) https://doi.org/10.1007/s10973-019-08324-3
14. Lu, D., Ramzan, M., Mohammad, M., Howari, F., Chung, J.D.: A thin film flow of nanofluid comprising carbon nanotubes influenced by Cattaneo-Christov heat flux and entropy generation. Coatings. **9**(5), 1–16 (2019). https://doi.org/10.3390/coatings9050296
15. Suleman, M., Ramzan, M., Ahmad, S., Lu, D., Muhammad, T., Chung, J.D.: A numerical simulation of silver–water nanofluid flow with impacts of Newtonian heating and homogeneous - heterogeneous reactions past a nonlinear stretched cylinder. Symm. **11**(2), 1–13 (2019). https://doi.org/10.3390/sym11020295
16. Suleman, M., Ramzan, M., Ahmad, S., Lu, D.: Numerical simulation for homogeneous–heterogeneous reactions and Newtonian heating in the silver-water nanofluid flow past a nonlinear stretched cylinder. Phys. Scr. **94**(8), 1–9 (2019) https://doi.org/10.1088/1402-4896/ab03a8
17. Madhu, M., Kishan, N., Chamkha, A.: Boundary layer flow and heat transfer of a non-Newtonian nanofluid over a non-linearly stretching sheet. Int. J. of Numer. Meth. for Heat & Fluid Flow. **26**(7), 2198–2217 (2016)
18. Madhu, M., Kishan, N.: Finite element analysis of heat and mass transfer by MHD mixed convection stagnation-point flow of a non-Newtonian power-law nanofluid towards a stretching surface with radiation. J. of the Egyp. Math. Soci. **24**(3), 458–470 (2016)
19. Macha, M., Naikoti, K., Chamkha, A.J.: MHD flow of a non-Newtonian nanofluid over a non-linearly stretching sheet in the presence of thermal radiation with heat source/sink. Eng. Comput. **33**(5), 1610–1626 (2016) https://doi.org/10.1108/EC-06-2015-0174
20. Alebraheem, J., Ramzan, M.: Flow of nanofluid with Cattaneo- Christov heat flux model. Appl. Nano- sci. 1–11 (2019)
21. Farooq, U., Lu, D.C., Munir, S., Suleman, M., Ramzan, M.: Flow of rheological nanofluid over a static wedge. J. of Nanofluids. **8**(6), 1362–1366 (2019)
22. Farooq, U., Lu, D., Munir, S., Ramzan, M., Suleman, M., Hussain, S.: MHD flow of Maxwell fluid with nanomaterials due to an exponentially stretching surface. Sci. reports. **9**(1), 1–11 (2019) https://doi.org/10.1038/s41598-019-43549-0
23. Macha, M., Reddy, C.S., Kishan, N.: Magnetohydrodynamic flow and heat transfer to Sisko nanofluid over a wedge. Int. J. of Fluid Mech. Res. **44**(1), (2017)
24. Aman, F., Ishak, A.: Mixed convection boundary layer flow towards a vertical plate with a convective surface boundary condition. Math. Prob. in Eng. **2012**, 1–11 (2012)
25. Mahanthesh, B., Gireesha, B.J., Gorla, R.S.R.: Heat and mass transfer effects on the mixed convective flow of chemically reacting nanofluid past a moving/stationary vertical plate. Alex. Eng. J. **55**, 569–581 (2016) https://doi.org/10.1016/j.aej.2016.01.022
26. Ahamed, S.M., Mondal, S., Sibanda, P.: Unsteady mixed convection flow through a permeable stretching flat surface with partial slip effects through MHD nanofluid using spectral relaxation method. Open Phys. **15**, 323–334 (2017)
27. Haroun, N.A.H., Sibanda, P., Mondal, S., Motsa, S.S.: On unsteady MHD mixed convection in a nanofluid due to a stretching/shrinking surface with suction/injection using the spectral relaxation method. Bound. Value Prob. **24**, 1–17 (2015). https://doi.org/10.1186/s 13661-015-0289-5
28. Haroun, N.A.H., Mondal, S., Sibanda, P.: Effects of thermal radiation on mixed convection in a MHD nanofluid flow over a stretching sheet using a spectral relaxation method. Int. J. of Math. Comput. Phys. Elec. Comp. Eng. **11**(2), 33–42 (2017)

29. Khan, A.Q., Rasheed, A.: Mixed convection magnetohydrodynamics flow of a nanofluid with heat transfer: a numerical study. Math. Prob. in Eng. **2019**, 1–14 (2019) https://doi.org/10.1155/2019/8129564
30. Reddy, C.R., Surender, O., Rao, C.V.: Effects of Soret, Hall and ion-slip on mixed convection in an electrically conducting Casson fluid in a vertical channel. Nonlinear Eng. **5**(3), 167–175 (2016)
31. Reddy, C.R., Surender, O., Rao, C.V., Pradeepa, T.: Adomian decomposition method for Hall and ion-slip effects on mixed convection flow of a chemically reacting Newtonian fluid between parallel plates with heat generation/absorption. Prop. Power Res. **6**(4), 296–306 (2017) https://doi.org/10.1016/j.jppr.2017.11.001
32. Srinivasacharya, D., Shafeeurrahaman, M.: Mixed convection flow of nanofluid in a vertical channel with hall and ion-slip effects. Front. in Heat Mass Transf. **8**(11), 1–8 (2017). https://doi.org/10.5098/hmt.8.11
33. Srinivasacharya, D., Shafeeurrahaman, M.: Hall and ion slip effects on mixed convection flow of nanofluid between two concentric cylinders. J. of the Assoc. of Arab Univ. for Basic Appl. Sci. **24**, 223–231 (2017) https://doi.org/10.1016/j.jaubasr.2017.03.002
34. Md. Shafeeurrahman, D. Srinivasacharya, Radiation effect on mixed convection flow of nanofluid between two concentric cylinders with Hall and Ion-slip effects, AAM: Int. J. Special Issue No. 4 (2019) 82 – 96.
35. Su, X.: Hall and ion-slip effects on the unsteady MHD mixed convection of $\overline{\text{Cu}}$-water nanofluid over a vertical stretching plate with convective heat flux. Indian J. of Pure Appl. Phys. **55**, 564–573 (2017)
36. Motsa, S.S., Shateyi, S.: The effects of chemical reaction, Hall, and ion-slip currents on MHD micropolar fluid flow with thermal diffusivity using a novel numerical technique. J. of Appl. Math. **2012**, 1–30 (2012). https://doi.org/10.1155/2012/689015
37. Bilal, M., Hussain, S., Sagheer, M.: Boundary layer flow of magneto-micropolar nanofluid flow with Hall and ion-slip effects using variable thermal diffusivity. Bull. of the polish acad. of sci. tech. sci. **65**(3), 383–390 (2017). https://doi.org/10.1515/bpasts-2017-0043
38. Ghara, N., Maji, S.L., Das, S., Jana, R., Ghosh, S.K.: Effects of Hall current and ion-slip on unsteady MHD Couette flow. Open J. of Fluid Dynam. **2**, 1–13 (2012) https://doi.org/10.4236/ojfd.2012.21001
39. Ali, F.M., Nazar, R., Arifin, N.M., Pop, I.: Effect of Hall current on MHD mixed convection boundary layer flow over a stretched vertical flat plate. Meccanica. **46**, 1103–1112 (2011). https://doi.org/10.1007/s11012-010-9371-3
40. Motsa, S.S., Makukula, Z.G.: On spectral relaxation method approach for steady von *Ka*€rma€n flow of a Rreiner-Rivlin fluid with Joule heating, viscous dissipation and suction/injection. Cent. Europ. J. Phys. **11**(3), 363–374 (2013). https://doi.org/10.2478/s11534-013-0182-8
41. Shateyi, S., Marewo, G.T.: A new numerical approach for the laminar boundary layer flow and heat transfer along a stretching cylinder embedded in a porous medium with variable thermal conductivity. J. of Appl. Math. **2013**, 1–7 (2013) https://doi.org/10.1155/2013/576453
42. Shateyi, S., Marewo, G.T.: A new numerical approach of MHD flow with heat and mass transfer for the UCM fluid over a stretching surface in the presence of thermal radiation. Math. Prob. in Eng. **2013**, 1–8 (2013) https://doi.org/10.1155/2013/670205
43. Ramzan, M., Bilal, M., Chung, J.D., Farooq, U.: Mixed convective flow of Maxwell nanofluid past a porous vertical stretched surface – an optimal solution. Results in Phys. **6**, 1072–1079 (2016) https://doi.org/10.1016/j.rinp.2016.11.036
44. L. N. Trefethen, Spectral methods in MATLAB. vol. 10 of *Software, Environments, and Tools*, SIAM, Philadelphia, Pa, U.S.A. (2000).
45. Grubka, L.J., Bobba, K.M.: Heat transfer characteristics of a continuous stretching surface with variable temperature. ASME J. Heat Transf. **107**, 248–250 (1985)

Publisher's Note

Springer Nature remains neutral with regard to jurisdictional claims in published maps and institutional affiliations.